

Mitigating Object Hallucinations in Large Vision-Language Models via Attention Calibration

Yunan Zhu¹, Linwei Tao¹, Minjing Dong², Chang Xu¹

¹University of Sydney

²City University of Hong Kong

{yzhu0986, linwei.tao, c.xu}@sydney.edu.au, minjdong@cityu.edu.hk

Abstract

Large Vision-Language Models (LVLMs) exhibit impressive multimodal reasoning capabilities but remain highly susceptible to object hallucination, where models generate responses that are not factually aligned with the visual content. Recent works attribute this issue to an inherent bias of LVLMs where vision token attention map has spurious focus on certain positions, and propose to mitigate this issue by reordering visual tokens. However, we find that different LVLMs exhibit different correlations between attention and spatial position, which makes the existing static solution difficult to generalize to other LVLMs. To begin with, we investigate the attention bias introduced by image tokens through a toy experiment, in which a blank image is fed into the model to capture its position-dependent bias. We then remove this bias from the original attention map, which already leads to a substantial reduction in hallucinations. This proof of concept validates the core intuition behind attention calibration. Building upon this insight, we propose Dynamic Attention Calibration (DAC)—a lightweight, plug-and-play module that leverages contrastive learning to dynamically enforce positional invariance. Unlike static baselines, DAC adapts to different models and inputs in a robust and learnable manner, offering a generalizable solution to mitigate attention-related hallucinations in LVLMs. Comprehensive experiments across multiple benchmarks demonstrate that DAC significantly reduces object hallucination while improving general multimodal alignment. Our method achieves state-of-the-art performance across diverse LVLM architectures on various metrics. Our code is available at <https://github.com/johnnynyn/attention-calibration>.

Introduction

Large Vision-Language Models (LVLMs) (Liu et al. 2024c; Bai et al. 2023; Dai et al. 2024; Zhu et al. 2023; Ye et al. 2024) have garnered significant attention in the AI research community for their remarkable ability to comprehend the visual world and engage in conversational interactions with humans. Despite these advances, LVLMs continue to face critical challenges, particularly in the form of object hallucination (Li et al. 2023a; Rohrbach et al. 2018; Cui et al. 2023), a phenomenon where models generate responses that are not factually aligned with the visual content. This issue undermines the reliability of LVLMs, posing a significant barrier to their deployment in real-world applications.

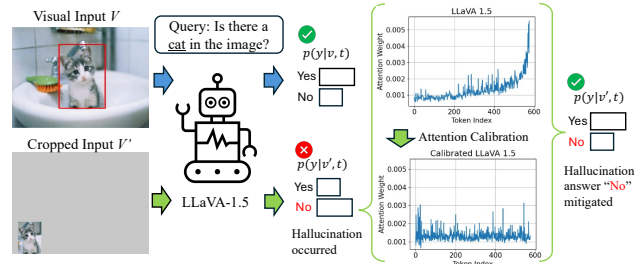


Figure 1: Illustration of Attention Calibration. The LVLM exhibits imbalanced perception of object spatial locations, failing to identify the object cat against an empty background. The hallucinated answer “No” (highlighted in red) is mitigated during inference by calibrating biased vision token attention

A variety of approaches have been proposed to mitigate object hallucination in LVLMs. One common strategy involves post-hoc correction using revisor models (Yin et al. 2023; Zhou et al. 2024; Lee et al. 2023), which aim to reduce hallucinated responses by refining outputs. Another approach improves supervised fine-tuning through diversified instruction tuning data (Liu et al. 2024a; Yu et al. 2024) or aligns model responses with human preferences (Sun et al. 2023). Recently, several studies have explored training-free methods for mitigating object hallucination by addressing issues in the autoregressive decoding process of LVLMs (Leng et al. 2023; Huo et al. 2024; Huang et al. 2023).

A recent study (Xing et al. 2024) reveals that LVLMs’ perception varies with object positions due to the inherent processing order in autoregressive models. As 2D vision tokens are concatenated with text tokens and flattened into a raster-scan sequence (top-to-bottom, left-to-right), the model develops a bias, prioritizing tokens in the bottom-right region closer to the instruction tokens (Figure 2a), termed as Spatial Perception Bias (SPB). This spatial bias skews perception capabilities. To mitigate this, Xing et al. (2024) propose a position alignment technique that reorders the perception sequence, reducing spatial bias.

However, this approach has two major limitations. First, the method is based on the assumption that the model assigns greater attention to tokens that are relatively nearby.

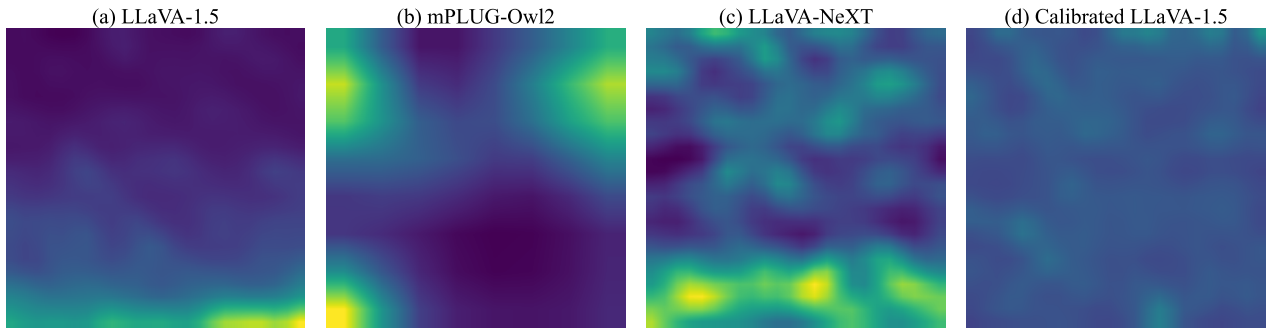


Figure 2: Spatial Position Bias influences how LVLMs perceive objects based on their position within an image. The visualization above illustrates vision token attention weights from the final token before output generation, during the decoding process for different models on a blank white image in response to the open-ended prompt: “Please describe this image in detail.” (a) shows LLaVA-1.5, which exhibits an increasing trend in attention distribution following a raster scan order, as identified by (Xing et al. 2024). (b-c) represent other models, displaying arbitrary attention distributions. (d) depicts the calibrated vision token attention map of LLaVA-1.5 after Dynamic Attention Calibration.

As demonstrated in Figure 2(a-c), our analysis reveals that the attention distributions of vision tokens vary significantly across different LVLm models and unexpectedly high attentions are assigned to arbitrary locations. This observation challenges the generalization of the heuristic reordering strategy proposed by Xing et al. (2024), highlighting the need for a more dynamic and adaptable solution. Second, the proposed technique requires retraining the entire network, which is computationally expensive and often impractical for large-scale LVLms, underscoring the necessity of developing a lightweight alternative.

Building on this analysis, we propose to mitigate object hallucination by calibrating the SPB in attention maps. As a proof of concept, Uniform Attention Calibration (UAC) subtracts a static bias extracted from the attention map of a blank image input and confirms that reducing SPB lowers hallucination. Motivated by this evidence, we further relax the assumption in UAC and introduce Dynamic Attention Calibration (DAC) to fine-tune LVLms for better generalization. Specifically, DAC consists of a learnable plug-and-play module integrated into the self-attention mechanism. With a simple yet effective data augmentation technique, the module is then fine-tuned via contrastive learning to encourage consistent outputs with different object positions in the image, which dynamically adjusts vision token attention map to tackle object hallucination.

Comprehensive experiments confirm the effectiveness of DAC, revealing substantial improvements across multiple object hallucination benchmarks for a range of LVLms, including LLaVA-1.5 (Liu et al. 2024c), mPLUG-Owl2 (Ye et al. 2024), and LLaVA-NeXT (Liu et al. 2024b). Additionally, our approach strengthens the overall perception capabilities of LVLms, as demonstrated by strong performance on MME (Fu et al. 2024) and LLaVA-Bench (Liu et al. 2024c). In summary, our main contributions are as follows:

1. We systematically investigate Spatial Perception Bias (SPB) in the attention mechanism of various LVLms,

revealing its strong correlation with object hallucination and its unpredictable nature across different models.

2. We propose Dynamic Attention Calibration (DAC), a lightweight, learnable, and plug-and-play module that dynamically adjusts vision token attention to robustly mitigate SPB.
3. Extensive experiments confirm that DAC significantly reduces object hallucination and enhances overall perception, achieving notable improvements across multiple LVLms and benchmarks.

Related Work

Visual-Language Models

Large Vision-Language Models (LVLms) have evolved from early BERT-based architectures (Devlin et al. 2018; Lu et al. 2019; Chen et al. 2019) to models that integrate Large Language Models (LLMs) (Bai et al. 2023; Brown et al. 2020; Gilardi, Alizadeh, and Kubli 2023; Raffel et al. 2020; Taori et al. 2023). Early vision-language models, such as ViLBERT (Lu et al. 2019) and LXMERT (Tan and Bansal 2019), fused visual and textual features through transformer-based architectures. The introduction of LLMs enabled contrastive learning approaches like CLIP (Radford et al. 2021) and ALIGN (Jia et al. 2021), improving multimodal adaptability. Recent LVLms, such as LLaVA (Liu et al. 2024c) and InstructBLIP (Dai et al. 2024), leverage visual instruction tuning for improved context-aware generation. Advances have further enabled referential dialogues (Chen et al. 2023a; You et al. 2023; Zhang et al. 2023a), interleaved image-text processing (Alayrac et al. 2022; Awadalla et al. 2023), and visual prompts (Peng et al. 2023; Zhang et al. 2023b; Chen et al. 2023b), broadening LVLm applications in interactive AI systems. These developments highlight a growing shift toward task-specific fine-tuning and multimodal interaction.

Hallucination in VLMS

Object hallucination arises when Large Vision-Language Models (LVLMs) generate textual descriptions containing objects or attributes not present in the accompanying image (Cui et al. 2023; Liu et al. 2024d; Guan et al. 2023; Li et al. 2023b; Wang et al. 2024; Nie et al. 2024). This phenomenon is frequently observed in tasks such as image captioning and visual question answering, where maintaining an accurate alignment between visual and textual content is critical. A range of methods has been proposed to address hallucination, from post-hoc correction using external or self-correcting models (Yin et al. 2023; Zhou et al. 2024; Lee et al. 2023) to enhanced instruction tuning that diversifies training data or aligns outputs with human feedback (Liu et al. 2024a; Yu et al. 2024; Sun et al. 2023). Recently, training-free approaches that rely on model-based distribution comparisons were proposed (Leng et al. 2023; Huo et al. 2024; Huang et al. 2023). As LVLMs grow more sophisticated and versatile, understanding and mitigating object hallucination remains a key focus in multimodal learning research. From a unique perspective, our design is rooted in the correlation between vision token attention and object hallucination.

Preliminary

In this section, we provide a brief overview of the widely adopted LVLMs architecture and explain how vision tokens are involved in the self attention module. Additionally, we review the how LVLMs exhibit spatial perception bias problem, highlighting systematic biases that affect LVLM hallucination.

LVLMs: Generation and Attention Mechanism

Vision and Language Inputs LVLMs process both image v and text t inputs. Raw images are divided into patches and encoded by a visual encoder, followed by a cross-modal projection module that maps visual features into the token space. This yields a sequence of vision tokens $v = \{v_i \mid i = 1, 2, \dots, n\}$, where n is the number of vision tokens. Text inputs are tokenized and embedded into text tokens $t = \{t_j \mid j = 1, 2, \dots, m\}$, where m is the number of text tokens. The vision and text tokens are then concatenated into a unified input sequence $x = \{v, t\}^1$, ensuring a shared multimodal representation space, with $v_i, t_j \in \mathbb{R}^d$, where d denotes the feature dimensionality.

Language Model Generation LVLMs are typically built on pre-trained LLMs such as Vicuna (Chiang, Li, and et al. 2023) or LLaMA (Touvron, Martin, and et al. 2023), parameterized by θ . The model takes a input x and predicts the next token probability $p(y_i)$ at time step i in an autoregressive manner:

$$p(y_i \mid x, y_{<i}) = \text{softmax}(\text{logit}_\theta(y_i \mid x, y_{<i})) \quad (1)$$

Self-Attention Mechanism The self-attention mechanism computes token relevance by projecting the output of previous layer into query Q , key K , and value V with linear

transformations W_Q, W_K, W_V . The self attention output is computed as

$$\text{SA}(Q, K, V) = \text{softmax}(\mathbf{A} + M) \cdot V, \quad \mathbf{A} = \frac{Q \cdot K^T}{\sqrt{d_l}}, \quad (2)$$

where $\mathbf{A} \in \mathbb{R}^{B \times H \times (n+m) \times (n+m)}$ denotes attention weight matrix, B and H represent the batch size, and number of attention heads, respectively. M denotes the causal mask, and d_l is the dimensionality of Q, K , and V . We denote \mathbf{A}^i as the attention matrix after i -th layer of LVLM. In this paper, we denote vision token attention $\mathbf{A}_{\text{img}} \in \mathbb{R}^{B \times H \times n}$ as the slice of the attention weights corresponding to the query from the last input token (the token immediately preceding the generated output) and the keys of all vision tokens v .

Spatial Perception Bias

When given a blank white image and the open-ended prompt “Please describe this image in detail”, LVLMs are expected to distribute attention uniformly across the entire image. However, as shown in Figure 2a, the self-attention module assigns varying levels of attention to different spatial regions. For instance, LLaVA-1.5 places greater attention on later visual tokens, particularly near the bottom-right. This systematic attention bias reflects position-dependent sensitivity to visual features. We define this phenomenon as Spatial Perception Bias (SPB)—a systematic error in the self-attention module that skews attention weights toward specific spatial regions, leading to perception inconsistencies.

Xing et al. (2024) were the first to identify a similar issue, attributing it to the long-term decay effect of position encoding. Specifically, LVLMs tend to assign lower attention to tokens corresponding to the top-left region of an image compared to those in the bottom-right region. This asymmetric attention makes LVLMs more susceptible to object hallucination in the top-left region, where visual grounding is weaker. To mitigate this, they proposed reordering the visual token sequence to achieve a more balanced attention distribution. However, when comparing Figure 2(a-c), we find that SPB varies significantly across models and can result in unexpectedly high attention to arbitrary locations. Consequently, a predefined token reordering strategy cannot generalize well to LVLMs beyond LLaVA-1.5.

Method

Uniform Attention Calibration

To understand the core issue of spatial position bias, we can consider a simplified scenario. We hypothesize that an ideal model, when presented with a meaningless image (e.g., a blank white image), should distribute its attention uniformly across all visual tokens. Any deviation from this uniformity can be interpreted as a form of inherent model bias.

This leads to a straightforward calibration strategy we term Uniform Attention Calibration (UAC). The core idea is to first measure the model’s vision token attention, $\hat{\mathbf{A}}_{\text{img}}$, on a meaningless input (we use a blank white image by default). From this, we compute a static calibration matrix, \mathbf{W} , designed to counteract the observed bias:

¹We omit the system tokens for simplicity.

$$\mathbf{W} = \frac{\text{avg}(\tilde{\mathbf{A}}_{\text{img}})}{\tilde{\mathbf{A}}_{\text{img}}} \quad (3)$$

where $\text{avg}(\cdot)$ denotes the average value over all elements of the matrix. During inference, this pre-computed matrix is applied as an affine transformation to the attention map of any given input image, \mathbf{A}_{img} , via an element-wise product:

$$\mathbf{A}'_{\text{img}} = \mathbf{W} \circ \mathbf{A}_{\text{img}} \quad (4)$$

By default, UAC is applied to a single self-attention layer in the decoder

Despite its simplicity, this approach serves as a valuable proof of concept. As shown in Table 1, we can observe that attention calibration effectively alleviate hallucination by mitigating SPB, particularly in the adversarial setting. This result supports our hypothesis that attention calibration is a promising direction. More results are provided in the Appendix.

However, the fundamental limitation of UAC remains its static, “one-size-fits-all” nature. Relying on a single bias profile is unlikely to work for diverse, content-rich inputs. Furthermore, such brute-force adjustments to the attention mechanism risk degrading the LVLM’s general performance on other tasks. This motivates the need for a more robust and adaptive solutions.

Dynamic Attention Calibration

To this end, we introduce Dynamic Attention Calibration (DAC). Instead of relying on a static calibration, DAC is a trainable, plug-and-play module designed to learn input-specific attention adjustments. It moves beyond a predefined rule by utilizing a contrastive learning framework (Wu et al. 2018; Chen et al. 2020) to ensure the model produces consistent outputs regardless of an object’s spatial position, thereby learning to mitigate SPB in a more effective and generalizable manner.

DAC Design Motivated by the superior calibration performance of affine transformation in the field of uncertainty calibration (Platt 1999), we introduce a lightweight trainable transformation f to calibrate unreliable vision token attention weights before SoftMax function as $\mathbf{A}'_{\text{img}} = f(\mathbf{A}_{\text{img}})$, where \mathbf{A}'_{img} denotes the calibrated vision token attention weights. Specifically, the transformation f operates within the self-attention mechanism of the transformer decoder layers and consists of a small stack of linear transformations with ReLU activations. The details about building blocks can be found in the Appendix. The forward pass of DAC module can be defined as

$$\begin{aligned} \mathbf{A}'_{\text{img}} &= f(\mathbf{A}_{\text{img}}) = \mathbf{g}_{L-1} \mathbf{W}_L + \mathbf{b}_L, \\ \mathbf{g}_i &= \text{ReLU}(\mathbf{g}_{i-1} \mathbf{W}_i + \mathbf{b}_i), \text{ for } i \in \{1, \dots, N-1\}, \end{aligned} \quad (5)$$

where L denotes the layer number in DAC module, $\mathbf{W}_i \in \mathbb{R}^{D_i \times D_i}$ denotes the weight matrix of layer i , $\mathbf{b}_i \in \mathbb{R}^{D_i}$ denotes the bias vector, \mathbf{g}_i represents the output of the i -th layer, and $\mathbf{g}_0 = \mathbf{A}_{\text{img}}$. The DAC module can be applied to any layer of the language model decoder, targeting the layers responsible for vision tokens processing.

DAC Optimization With the DAC module in Eq. 5, a much stronger constraint can be imposed on vision token attention weights of LVLMs to alleviate the bias. Instead of the uniform constraint in UAC, we further propose to force the consistent outputs wherever the object locates in the image. The key idea is to ensure that the model maintains the same capability of identifying an object regardless of its position within the image. However, to impose such a constraint, it could be challenging to obtain sufficient training data variants with different object positions. Thus, we introduce a simple yet effective data augmentation technique inspired by the concept of instant discrimination (Wu et al. 2018; Chen et al. 2020).

Formally, we randomly select 100 images from MSCOCO as our validation set, denoted as \mathcal{D}_{val} . Each image $V \in \mathcal{D}_{\text{val}}$ is paired with ground-truth annotations and their corresponding bounding boxes. The validation set \mathcal{D}_{val} undergoes an augmentation process to produce the augmented calibration dataset \mathcal{D}_{cal} . Specifically, we crop the ground truth objects from the images using the annotations and bounding boxes provided, then apply random resizing and paste the cropped objects onto a pure white background as V_{crop} . For each V_{crop} , we generate balanced positive and negative query-label pairs, ensuring a well-balanced dataset. Additionally, we include annotations for the cropped images V_{crop} to be utilized in instance discrimination tasks, as discussed later in the paper. The detailed augmentation process is summarized in the Appendix.

With sufficient augmented data from \mathcal{D}_{cal} , we propose leveraging contrastive learning to encourage LVLMs to focus on objects themselves rather than their absolute positions in the image. This approach ensures consistent outputs regardless of object position. By reducing reliance on positional cues, the model learns to robustly identify objects despite spatial transformations. Specifically, contrastive learning is formulated to increase the similarity between embeddings of the same object at different spatial locations while pushing apart the embeddings of different objects. We begin with an \mathcal{D}_{cal} dataset and randomly sample a minibatch of B examples. Each example then undergoes an additional augmentation process, resulting in a total of $2B$ augmented data points. Following the approach of (Wu et al. 2018), for each positive pair, we consider the remaining $2(B-1)$ augmented examples within the minibatch as negative examples. Given the embeddings z_i and z_j of the positive augmented pair \tilde{v}_i and \tilde{v}_j , the contrastive loss can be expressed as:

$$\ell_{\text{CL}}(i, j) = -\log \frac{\exp(\text{sim}(\mathbf{z}_i, \mathbf{z}_j)/\tau)}{\sum_{k=1}^{2B} \mathbf{1}_{[k \neq i]} \exp(\text{sim}(\mathbf{z}_i, \mathbf{z}_k)/\tau)}, \quad (6)$$

where B denotes the number of examples in a minibatch, $\text{sim}(\cdot, \cdot)$ represents the cosine similarity, $\mathbf{1}_{[k \neq i]}$ is an indicator function, and τ is the temperature parameter. Combined

Algorithm 1: DAC’s Main Learning Algorithm

Input: Batch size B , constant τ , frozen backbone networks $f(\cdot)$ and projection head $g(\cdot)$, augmentation distribution \mathcal{T} , calibration set $\mathcal{D}_{\text{cal}} = \{(T_{\text{cal}}, V_{\text{crop}}, Y_{\text{cal}})\}$
for sampled minibatch $\{(t_k, v_k, y_k)\}_{k=1}^B \in \mathcal{D}_{\text{cal}}$ **do**
 for all $k \in \{1, \dots, B\}$ **do**
 Draw one augmentation function $t \sim \mathcal{T}$
 # Original augmentation
 $\tilde{v}_{2k-1} = v_k$
 $z_{2k-1} = f(\tilde{v}_{2k-1})$ # Representation
 $\tilde{y}_{2k-1} = g(z_{2k-1})$ # Prediction
 $y_{2k-1} = y_k$ # Label
 # The second augmentation
 $\tilde{v}_{2k} = t(v_k)$
 $z_{2k} = f(\tilde{v}_{2k})$ # Representation
 $\tilde{y}_{2k} = g(z_{2k})$ # Prediction
 $y_{2k} = y_k$ # Label
 end for
 for all $i \in \{1, \dots, 2B\}$ and $j \in \{1, \dots, 2B\}$ **do**
 $s_{i,j} = z_i^\top z_j / (\|z_i\| \|z_j\|)$ # Pairwise similarity
 end for
 Compute the losses using:
$$\mathcal{L} = \mathcal{L}_{\text{CE}} + \lambda \cdot \mathcal{L}_{\text{CL}}$$

 Update DAC parameters to minimize \mathcal{L}
end for
Return: Fine-tuned DAC

with a cross-entropy (CE) loss, the final loss function is formulated as

$$\mathcal{L} = \mathcal{L}_{\text{CE}}(F(T_{\text{crop}}, V_{\text{crop}}), Y_{\text{crop}}) + \lambda \mathcal{L}_{\text{CL}}, \quad (7)$$

where F represents the model, T_{crop} and V_{crop} are the query and cropped image, Y_{crop} is the corresponding label, and λ is a hyperparameter balancing the two losses. We optimize our DAC using Eq. 7 alongside instruction tuning, while keeping all other components frozen. The overall training process is summarized in Algorithm 1.

Experiment

Setup

Models and Baselines We implement three representative LVLMs for evaluation: LLaVA-1.5 (Shang, Cai et al. 2024), mPLUG-Owl2 (Ye et al. 2024), and LLaVA-NeXT (Liu et al. 2024b) at the 7B scale. Our methods are compared against five methods. Baseline responses are generated using the original LVLMs, while other techniques such as Visual Contrastive Decoding (VCD) (Leng et al. 2023), OPERA (Huang et al. 2023), Self-Introspective Decoding (SID) (Huo et al. 2024), and Concentric Causal Attention (CCA) (Xing et al. 2024) are included for comparative analysis. We adopt the default settings for OPERA, VCD, and SID. For CCA, we directly use the provided weights. For each compared method, except OPERA, which uses beam search (beam size 5), we use greedy decoding for polling-based tasks (POPE and MME), and nucleus sampling ($p =$

1) for open-ended generation tasks (CHAIR and LLaVA-Bench).

Experiment Settings Unless otherwise specified, we integrate the DAC module into two consecutive layers of the language model decoder. For all tasks, we use a fixed validation set D_{val} , composed of 100 randomly selected MSCOCO images disjoint from any test set. For each image, we select up to three ground truth objects; if an image contains fewer than three objects, all available objects are included. Using these ground truth objects, we generate 10 cropped images per object, resulting in a dataset of approximately 5.4K (T, V, Y) pairs. By default, the contrastive loss strength λ is set to 0.01. To configure the DAC layer, we define 2–4 candidate layer buckets and select the setting when validation on D_{val} is applicable; otherwise, we adopt the same setting as used in the POPE MSCOCO Random.

For LLaVA-1.5, we fine-tune the DAC module on the D_{cal} dataset using a learning rate of 3×10^{-6} , a batch size of 8, and gradient accumulation steps of 4. The training takes approximately 40 minutes on two NVIDIA RTX 4090 GPUs. We apply attention calibration to the vision token attention \mathbf{A}_{img} , computed with the last input token as the query. Additional experimental details can be found in the Appendix.

Evaluation Results

POPE Polling-based Object Probing Evaluation (POPE) (Li et al. 2023a) is a method designed to assess object hallucination in LVLMs. It evaluates model performance by querying the presence of specific objects in images using yes-or-no questions. POPE employs three strategies for sampling negative objects: Random, Popular, and Adversarial (refer to (Li et al. 2023a) for details). Our evaluation utilizes two datasets: MSCOCO (Lin et al. 2014) and A-OKVQA (Schwenk et al. 2022). For each evaluation setup, every subset includes 3,000 questions across 500 images, resulting in a total of 18,000 yes-or-no questions. The evaluation pivots on two key metrics: Accuracy and the F1 score. DAC achieves the highest accuracy and F1 scores across most datasets and sampling setups, as shown in Table 2. Specifically, DAC delivers an average improvement of 1.01% in accuracy and 0.74% in F1 score for Random sampling, 2.19% in accuracy and 1.49% in F1 score for Popular sampling, and 2.41% in accuracy and 1.13% in F1 score for Adversarial sampling, compared to the next best existing approach. Notably, DAC achieves the largest accuracy gain in the more challenging Adversarial setting by effectively suppressing spurious visual cues that are unrelated to the target object.

CHAIR The Caption Hallucination Assessment with Image Relevance (CHAIR) metric (Rohrbach et al. 2018) is specifically designed to assess object hallucinations in image captioning tasks. CHAIR quantifies the degree of hallucinations in a generated image caption by calculating the proportion of objects mentioned in the caption that are not present in the ground truth label pool. Two common variants of CHAIR are defined: C_S and C_I , which measure hallucination at the instance and sentence levels, respectively. These metrics are formulated as follows:

$$C_S = \frac{|\text{hallucinated objects}|}{|\text{all mentioned objects}|}, \quad C_I = \frac{|\text{captions with hallucinated objects}|}{|\text{all captions}|}$$

Setting			Random		Popular		Adversarial		
Dataset	Model	Method	Accuracy↑	F1 Score↑	Accuracy↑	F1 Score↑	Accuracy↑	F1 Score↑	
MSCOCO	LLaVA-1.5	Baseline	89.63	89.74	86.23	86.82	79.70	81.71	
		VCD	87.53	87.81	84.43	85.20	78.13	80.38	
		OPERA	89.87	89.95	86.30	86.88	79.77	81.77	
		SID	89.43	89.08	85.93	85.94	80.43	81.47	
		CCA ²	89.77	89.05	86.45	86.02	83.97	83.82	
		DAC	90.83	90.60	89.50	89.10	84.12	84.42	
	mPLUG-Owl2	Baseline	86.27	86.88	80.73	82.52	76.17	77.69	
		VCD	84.40	84.79	81.00	81.12	77.10	77.00	
		OPERA	86.23	86.84	80.70	82.48	76.87	78.01	
		SID	86.30	86.86	81.27	82.82	77.27	79.89	
		DAC	87.71	87.57	84.96	84.46	82.58	82.32	
		LLaVA-NeXT	Baseline	91.27	90.76	88.60	88.27	85.50	85.54
	VCD		91.30	90.80	88.63	88.31	85.53	85.58	
	OPERA		91.36	90.80	88.65	88.60	85.10	85.75	
	SID		91.20	90.73	88.60	88.30	85.87	85.89	
	DAC		91.63	91.32	89.27	89.14	86.00	85.71	
	A-OKVQA		LLaVA-1.5	Baseline	87.30	88.49	80.30	83.21	69.33
		VCD		85.00	86.49	77.50	81.07	67.90	75.01
OPERA		87.27		88.50	80.47	83.38	69.20	76.09	
SID		87.30		88.00	82.00	83.80	72.93	77.48	
CCA		90.00		90.11	85.45	85.01	74.77	78.32	
DAC		89.70		90.33	83.96	85.52	75.42	79.21	
mPLUG-Owl2		Baseline	81.57	83.89	75.97	79.98	67.37	74.63	
		VCD	82.53	84.16	75.70	79.21	68.80	74.85	
		OPERA	81.53	83.86	75.93	79.94	67.30	74.58	
		SID	83.53	85.28	77.47	80.89	68.93	75.43	
		DAC	86.56	87.24	82.83	83.47	75.88	77.78	
		LLaVA-NeXT	Baseline	91.80	92.07	87.17	88.13	77.47	80.87
VCD	91.80		92.07	87.20	88.15	77.53	80.90		
OPERA	91.77		92.03	87.20	88.15	77.21	80.62		
SID	91.73		92.01	86.87	87.88	77.33	80.77		
DAC	92.37		92.47	89.13	89.62	78.80	81.56		

Table 2: POPE results. All results use greedy decoding, except OPERA (beam search), and are either reported from prior work or re-implemented using official code. Best performance in each setting is shown in **bold**.

Lower values of C_S and C_I indicate better performances. Following (Huang et al. 2023; Huo et al. 2024), we randomly select 500 images from MSCOCO validation set and query LVLMs using the prompt: “Please describe this image in detail.” To ensure a fair evaluation, we limit the maximum number of new tokens to 512 when generating descriptions. As shown in Table 3, our method demonstrates effective improvements. Notably, on C_S , DAC achieves a significant 38.14% improvement across models compared to the next best approach. The superior performance of our method on CHAIR metrics highlights its effectiveness in mitigating hallucinations in open-ended generation settings.

MME The MME benchmark (Fu et al. 2024) provides a comprehensive framework for evaluating LVLMs across

multiple dimensions. It includes ten perception-related subtasks and four cognition-focused tasks. Following (Leng et al. 2023; Yin et al. 2023), we evaluate four perception subtasks that assess object-level and attribute-level hallucinations, specifically measuring object existence, count, position, and color. Table 4 presents the performance of our method, DAC, on the MME hallucination subset using LLaVA-1.5. DAC achieves a notable improvement of 16.16% over the baseline and 2.34% over the current state-of-the-art hallucination mitigation approaches, demonstrating its effectiveness in enhancing the general perception capabilities of LVLMs.

GPT4V-Aided Evaluation We evaluate our approach on LLaVA-Bench (Liu et al. 2024c), a benchmark comprising 30 images paired with a total of 90 questions. LLaVA-Bench is designed to assess the ability of models to generate coher-

²CCA is only applicable for LLaVA-1.5

Setting	LLaVA-1.5		LLaVA-NeXT	
	$C_S \downarrow$	$C_I \downarrow$	$C_S \downarrow$	$C_I \downarrow$
Baseline	51.3	16.8	42.6	14.1
VCD	48.0	14.3	41.3	12.9
OPERA	45.2	12.7	39.4	11.8
SID	45.0	11.7	38.4	11.4
CCA	48.6	13.4	-	-
DAC	30.6	12.3	21.4	10.2

Table 3: CHAIR results on 500 randomly sampled MSCOCO images with a maximum sequence length of 512 tokens. All results use nucleus sampling ($p = 1$), except OPERA (beam search).

Setting	Object-level		Attribute-level		Total \uparrow
	$existence \uparrow$	$count \uparrow$	$position \uparrow$	$color \uparrow$	
Baseline	175.67	124.67	114.00	151.00	565.33
VCD	184.66	138.33	128.67	153.00	604.66
OPERA	180.67	133.33	123.33	155.00	592.33
SID	190.00	148.33	128.33	175.00	641.66
CCA	190.00	148.33	128.33	175.00	641.66
DAC	195.00	158.33	133.33	170.00	656.67

Table 4: MME hallucination subset results. All results use greedy decoding, except OPERA (beam search).

ent and contextually accurate responses for vision-language tasks. It categorizes questions into three types: conversation, detailed description, and complex reasoning. Following prior works (Liu et al. 2024c; Huang et al. 2023), we prompt these models to generate responses and use the text-only GPT-4 (Achiam et al. 2023) as the judge to rate these responses. The results on LLaVA-1.5 are presented in Table 5. Our method demonstrates strong performance across all question type. These results highlight the effectiveness of our approach at preserving language understanding and generation capabilities while significantly mitigating object hallucination.

Ablation Study

Hyperparameter We analyzed two key hyperparameters: the contrastive loss strength λ and the decoder layers N_{DAC} to which DAC is applied. As shown in Figure 3, DAC consistently outperforms the baseline across most settings.

The contrastive learning component is critical for achieving performance gains. Our ablation study clearly demonstrates this: when the component is removed entirely by setting $\lambda = 0$, the model is fine-tuned only on the CE loss and yields the lowest performance among all tested settings. While excessively high values can degrade generative capabilities, performance is stable across a range of settings near the optimum. Our experiments indicate that $\lambda = 0.01$ achieves the best performance, with negligible differences for nearby values. For consistency, we adopt $\lambda = 0.01$ for all experiments.

Our method offers flexibility in choosing the decoder lay-

Method	Complex \uparrow	Details \uparrow	Conv \uparrow	Average \uparrow
Baseline	66.3	46.7	68.7	60.6
VCD	69.6	51.6	57.3	61.6
OPERA	66.4	56.9	44.0	61.3
SID	66.7	51.3	66.3	60.4
CCA	66.1	53.9	69.4	64.3
DAC	70.3	50.0	72.7	64.3

Table 5: LLaVA-Bench results. The results are re-implemented using nucleus sampling ($p = 1$), except OPERA (beam search), based on the official code and evaluated with the latest available text-only GPT-4 API. Scores are normalized by the total possible score.

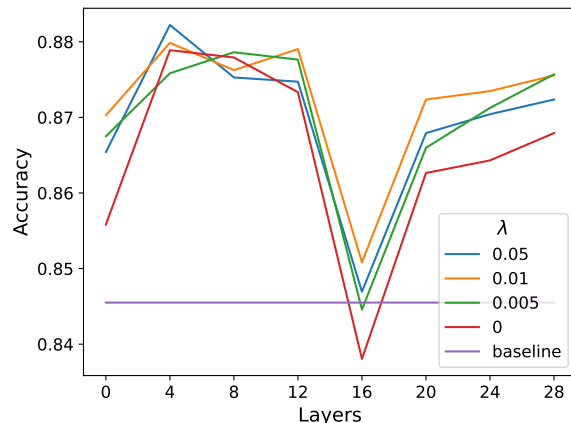


Figure 3: Performance of DAC under different settings of the hyperparameters λ and N_{DAC} . The x-axis indicates the starting N_{DAC} , with DAC applied to two consecutive layers. Each line corresponds to a different value for the contrastive strength, λ . The y-axis shows the average accuracy on the POPE MSCOCO benchmark using LLaVA-1.5

ers for applying the contrastive loss. Our results show that there is a wide range of effective choices. In practice, we follow a standard procedure: we identify 2–4 candidate pairs of consecutive decoder layers (e.g., layers 4–5 or 20–21) as brackets and select the best setting based on validation performance on D_{val} , if applicable.

Conclusion and Limitation

This paper investigates object hallucination in LVLMs and identifies SPB as a key contributor, characterized by an imbalance in vision token attention that causes unequal focus across spatial regions and varies across models. This bias distorts object perception, amplifies sensitivity to misleading visual cues, and increases the risk of hallucination, compromising reliability in real-world settings. A straightforward UAC experiment confirms that mitigating SPB effectively reduces hallucination. Building on this, we introduce DAC, a learnable module that dynamically refines attention weights within the self-attention mechanism. Extensive evaluation

confirms that DAC reduces hallucinations and enhances perception, highlighting attention calibration as a promising mitigation strategy.

Limitation While DAC is data-efficient in addressing SPB, its performance may be limited when validation data is scarce. Future work could explore data-free calibration and extend attention calibration to improve LLMs reliability.

Appendix

Additional UAC results

Setting	POPE MSCOCO			CHAIR		MME↑
	Rnd↑	Pop↑	Adv↑	C_S ↓	C_i ↓	
Baseline	89.7	86.8	81.7	51.3	16.8	565.3
VCD	87.8	85.2	80.4	48.0	14.3	604.7
OPERA	90.0	86.9	81.8	45.2	12.7	592.3
SID	89.1	85.9	81.5	45.0	11.7	641.7
CCA	89.1	86.0	83.8	48.6	13.4	641.7
UAC	90.2	87.6	83.7	49.0	14.9	638.3
DAC	90.6	89.1	84.4	30.8	12.7	656.7

Table 6: Results on POPE MSCOCO, CHAIR, and MME hallucination subsets. ‘‘Rnd’’ ‘‘Pop’’ and ‘‘Adv’’ represent the Random, Popular, and Adversarial settings, respectively. On POPE MSCOCO, results are reported as F1 scores. The best performances within each settings are highlighted in **bold**.

To address the SPB inherent in LVLMs, we propose a toy example method Uniform Attention Calibration (UAC). UAC recalibrates biased attention by estimating SPB from a meaningless input. We evaluate this method using LLaVA-1.5 on the POPE MSCOCO, CHAIR, and MME benchmarks, following the same experimental setup as in our other comparisons. As summarized in tab:pope-wrap, UAC achieves the best overall performance on POPE MSCOCO compared to current state-of-the-art methods, surpassing other training-free approaches by a substantial margin. On the MME dataset, UAC attains competitive results. However, on the open-ended generation benchmark CHAIR, UAC falls short of the top performers. We attribute this to its reliance on a single meaningless image bias for calibration, which, while effective for structured tasks, may degrade generation quality in open-ended settings by limiting the model’s ability to adapt to diverse contextual variations.

DAC architecture

Detailed Dynamic Attention Calibration(DAC) applied to each layer of vision token attention is shown in Figure 4.

Detailed Experimental Settings

Following the setup described in the main paper, we fix the contrastive-loss weight at $\lambda = 0.01$. The learning rates are set to 3×10^{-6} for LLaVA-1.5, 4×10^{-5} for MPLUG-Owl2, and 8×10^{-7} for LLaVA-Next. Implementation details for N_{DAC} on POPE are provided in Table 7, while those for CHAIR, MME, and LLaVA-Bench are listed in Table 8.

The application of DAC varies across models. For LLaVA-1.5 and LLaVA-NeXT, DAC is applied to the last token before prediction. For mPLUG-Owl2, DAC is applied to all tokens except system tokens, i.e., after the image starting position. For LLaVA-1.5 and LLaVA-NeXT, DAC consists of two layers with a hidden dimension of 576, which

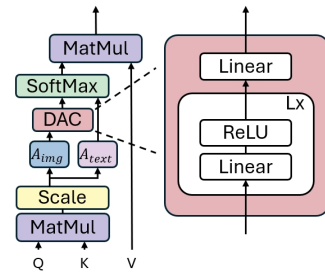


Figure 4: The Dynamic Attention Calibration (DAC) architecture consists of a small stack of linear transformations with ReLU activation, operating within the self-attention mechanism of transformer decoder layers to calibrate vision tokens attention.

Model	Parameters	POPE		
		Rnd	Pop	Adv
LLaVA-1.5	MSCOCO	20, 21	4, 5	4, 5
	AOKVQA	20, 21	4, 5	4, 5
MPLUG-Owl2	MSCOCO	12, 13	12, 13	12, 13
	AOKVQA	12, 13	12, 13	12, 13
LLaVA-NeXT	MSCOCO	16, 17	16, 17	16, 17
	AOKVQA	28, 29	28, 29	28, 29

Table 7: Optimal settings of DAC applied layers N_{DAC} on POPE evaluation. ‘‘Rnd’’ ‘‘Pop’’ and ‘‘Adv’’ represent the Random, Popular, and Adversarial settings, respectively.

matches both the input and output dimensions. For mPLUG-Owl2, DAC is set to three layers with a hidden dimension of 576 to maintain a similar capacity.

Different Sampling Strategies

Table 9 presents an ablation study on various sampling strategies conducted on the POPE-Random dataset using LLaVA-1.5. In addition to the greedy decoding baseline discussed in the main paper, the study evaluates five alternative strategies: Top-P sampling ($p = 0.9$ and $p = 1$), Top-K sampling ($k = 50$), Top-K sampling with temperature scaling ($k = 50$, temperature = 0.7), and direct sampling (temperature = 1). The results show that applying DAC consistently reduces hallucination and enhances overall model performance across all decoding methods, underscoring the robustness and generalizability of DAC in mitigating hallucinations under diverse sampling conditions.

Data Augmentation Process

The augmentation process consists of the following steps:

- For each annotated object in V :
 - Crop the region defined by its bounding box.
 - Randomly resize the cropped object to a minimum size of $(H/14) \times (W/14)$ pixels (the typical size of an image patch) and a maximum size of $(H/2) \times (W/2)$,

Model	CHAIR	MME	LLaVA-Bench
LLaVA-1.5	5, 6	20, 21	20, 21

Table 8: Optimal settings of DAC applied layers N_{DAC} on CHAIR, MME, and LLaVA-Bench using LLaVA-1.5.

Setting	Baseline		VCD		DAC	
	Acc \uparrow	F1 \uparrow	Acc \uparrow	F1 \uparrow	Acc \uparrow	F1 \uparrow
Top- $p = 0.9$	84.91	83.05	87.82	87.31	88.60	88.18
Top- $p = 1.0$	84.77	82.28	86.84	86.83	87.77	87.50
Top- $k = 50$	83.04	81.05	87.49	86.92	87.57	87.19
Top- $k, t = 0.7$	85.17	83.38	85.13	85.94	89.47	89.23
Sample, $t = 1$	83.29	81.33	87.73	87.16	88.17	87.86

Table 9: Various sampling strategies conducted on the POPE-Random dataset using LLaVA-1.5.

Algorithm 2: Data Augmentation Algorithm

Input: Calibration set $\mathcal{D}_{\text{cal}} = \{(T_i, V_i, Y_i)\}_{i=1}^I \subset \mathcal{D}_{\text{val}}$
 I : Size of calibration set
 J : Number of annotations per image
 K : Number of crops per object
Augmented set $\mathcal{D}_{\text{aug}} = \{\}$
for $i = 1$ to I **do**
 for $j = 1$ to J **do**
 for $k = 1$ to K **do**
 Get V_{crop} for object j
 Assign $(T_{\text{pos}}, V_{\text{crop}}, Y_{\text{pos}})$
 Assign $(T_{\text{neg}}, V_{\text{crop}}, Y_{\text{neg}})$
 Append both pairs to \mathcal{D}_{aug}
 end for
 end for
end for
Return: $\mathcal{D}_{\text{aug}} = \{(T_{\text{aug}}, V_{\text{crop}}, Y_{\text{aug}})\}$ with size $I \cdot J \cdot K \cdot 2$

where H and W are the height and width of the original image V .

- Replace the background of the cropped object with pure white, resulting in V_{crop}
- For each cropped object V_{crop} :
 - Generate a corresponding positive query T_{pos} that describes the cropped object and assign the label $Y_{\text{pos}} = \text{yes}$. Obtaining positive query-label pair: $(T_{\text{pos}}, V_{\text{crop}}, Y_{\text{pos}})$
 - Generate a ground-truth negative query T_{neg} , which refers to an object not present in the image, and assign the label $Y_{\text{neg}} = \text{no}$. Obtaining negative query-label pair: $(T_{\text{neg}}, V_{\text{crop}}, Y_{\text{neg}})$
 - Each cropped image V_{crop} results in one positive query-label pair and one negative query-label pair, ensuring a balanced augmented set.

Let I represent the number of original images in the calibration set \mathcal{D}_{cal} , J represent the average number of annotated ground-truth objects per image V , and K represent the

number of crops generated per object. The total size of the augmented dataset is: Total size of $\mathcal{D}_{\text{aug}} = I \cdot J \cdot K \cdot 2$

SPB on other blank images

Additional case studies of SPB under different vision and prompt inputs using LLaVA-1.5 are presented in Figures 5–11.

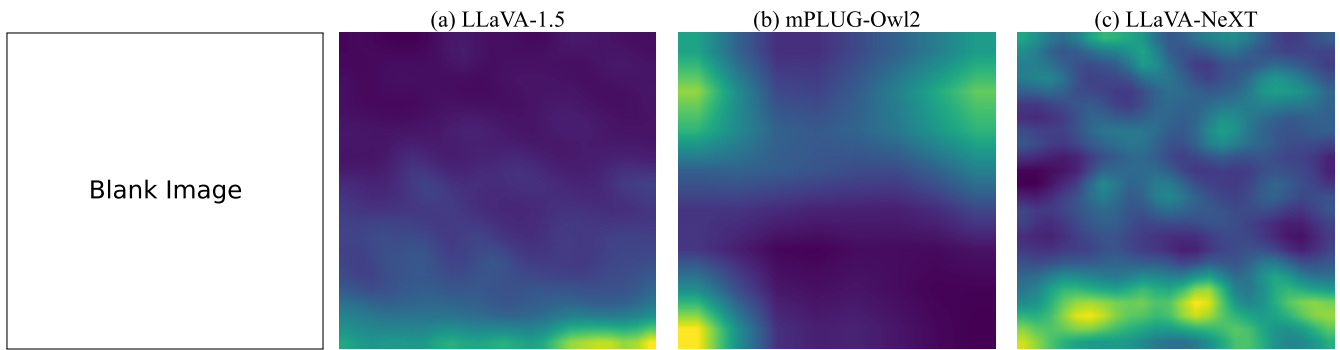


Figure 5: Vision tokens attention weights during the decoding process for different models on a blank white image in response to the polling prompt: “Is there a bear in the image?”

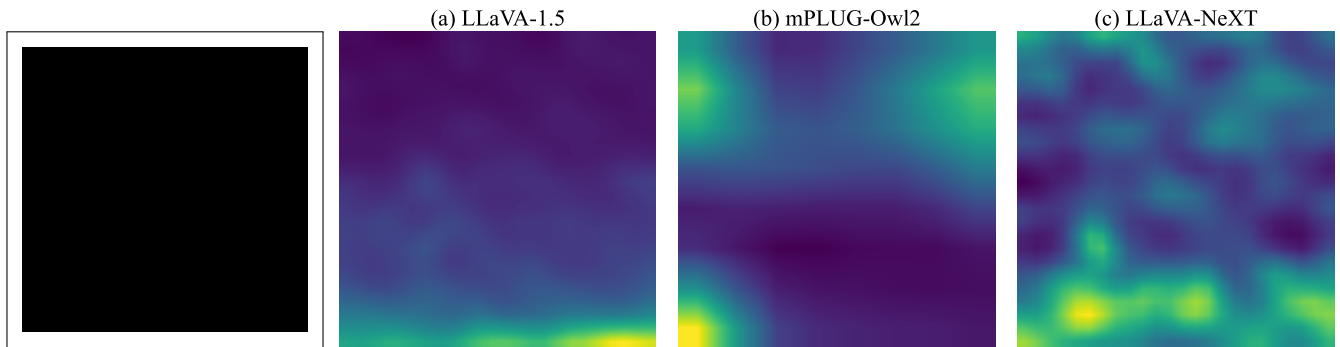


Figure 6: Vision tokens attention weights during the decoding process for different models on a blank black image in response to the polling prompt: “Is there a bear in the image?”

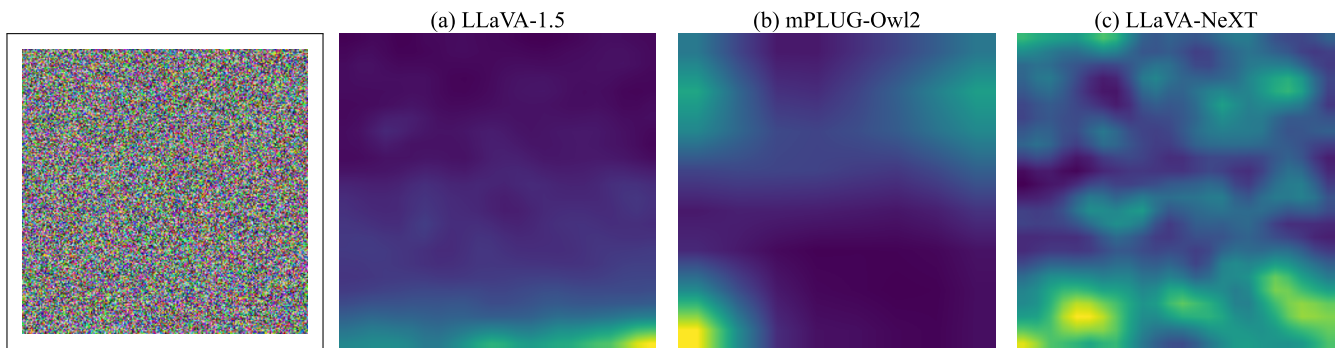


Figure 7: Vision tokens attention weights during the decoding process for different models on a blank noise image in response to the polling prompt: “Is there a bear in the image?”

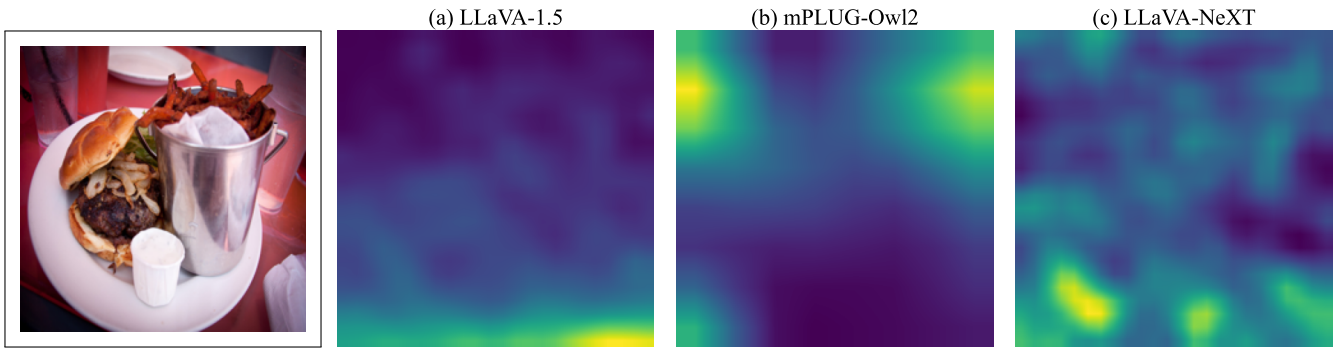


Figure 8: Vision tokens attention weights during the decoding process for different models on an actual image in response to the polling prompt: “Is there a bear in the image?”

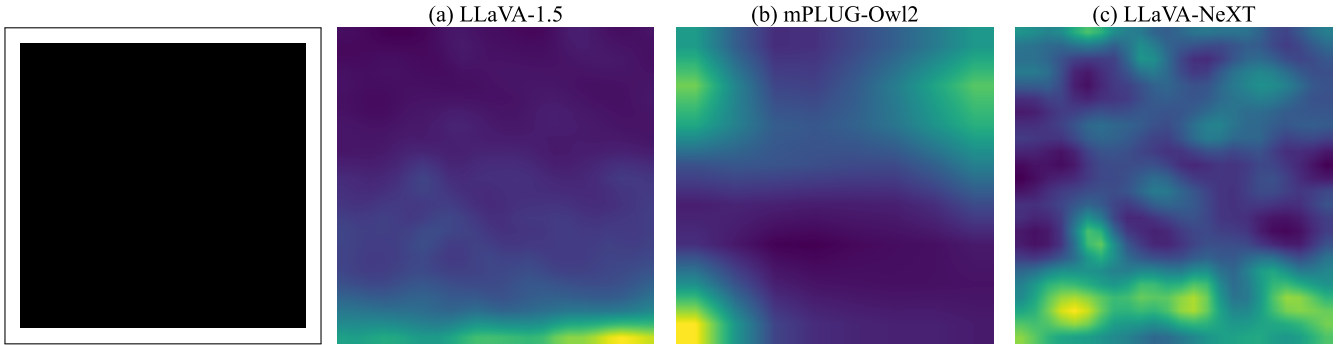


Figure 9: Vision tokens attention weights during the decoding process for different models on a blank black image in response to the open-ended prompt: “Please describe this image in detail.”

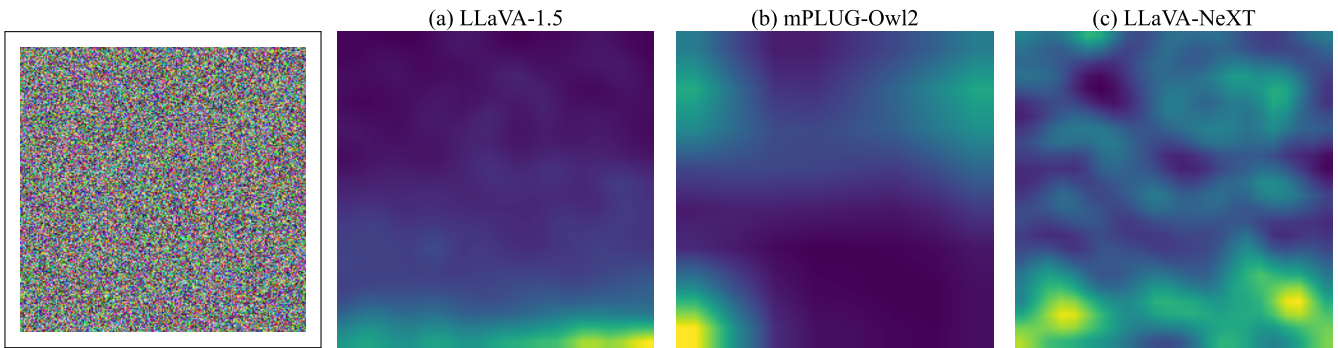


Figure 10: Vision tokens attention weights during the decoding process for different models on a blank noise image in response to the open-ended prompt: “Please describe this image in detail.”

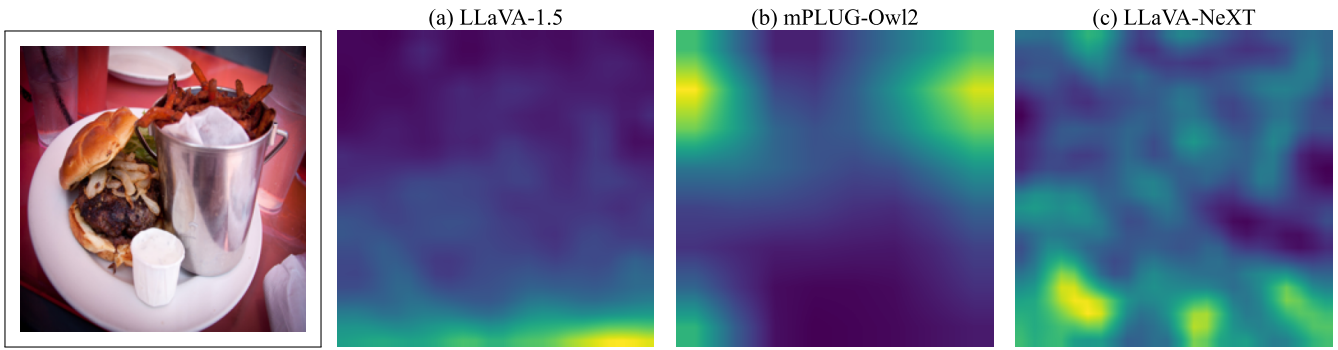


Figure 11: Vision tokens attention weights during the decoding process for different models on an actual image in response to the open-ended prompt: "Please describe this image in detail."

References

- Achiam, J.; Adler, S.; Agarwal, S.; Ahmad, L.; Akkaya, I.; Aleman, F. L.; Almeida, D.; Altenschmidt, J.; Altman, S.; Anadkat, S.; et al. 2023. GPT-4 Technical Report. *arXiv preprint arXiv:2303.08774*.
- Alayrac, J.-B.; Donahue, J.; Luc, P.; Miech, A.; Barr, I.; Hasson, Y.; Lenc, K.; Mensch, A.; Millican, K.; Reynolds, M.; et al. 2022. Flamingo: A Visual Language Model for Few-Shot Learning. *Advances in Neural Information Processing Systems*, 35: 23716–23736.
- Awadalla, A.; Gao, I.; Gardner, J.; Hessel, J.; Hanafy, Y.; Zhu, W.; Marathe, K.; Bitton, Y.; Gadre, S.; Sagawa, S.; et al. 2023. OpenFlamingo: An Open-Source Framework for Training Large Autoregressive Vision-Language Models. *arXiv preprint arXiv:2308.01390*.
- Bai, J.; Bai, S.; Chu, Y.; Cui, Z.; Dang, K.; Deng, X.; Fan, Y.; Ge, W.; Han, Y.; Huang, F.; et al. 2023. Qwen Technical Report. *arXiv preprint arXiv:2309.16609*.
- Brown, T.; Mann, B.; Ryder, N.; Subbiah, M.; Kaplan, J. D.; Dhariwal, P.; Neelakantan, A.; Shyam, P.; Sastry, G.; Askell, A.; et al. 2020. Language Models are Few-Shot Learners. In *Advances in Neural Information Processing Systems (NeurIPS)*, volume 33, 1877–1901.
- Chen, K.; Zhang, Z.; Zeng, W.; Zhang, R.; Zhu, F.; and Zhao, R. 2023a. Shikra: Unleashing Multimodal LLM’s Referential Dialogue Magic. *arXiv preprint arXiv:2306.15195*.
- Chen, T.; Kornblith, S.; Norouzi, M.; and Hinton, G. 2020. A Simple Framework for Contrastive Learning of Visual Representations. In *International Conference on Machine Learning*, 1597–1607. PMLR.
- Chen, W.-G.; Spiridonova, I.; Yang, J.; Gao, J.; and Li, C. 2023b. LLaVA-Interactive: An All-in-One Demo for Image Chat, Segmentation, Generation and Editing. *arXiv preprint arXiv:2311.00571*.
- Chen, Y.-C.; Li, L.; Yu, L.; Kholy, A. E.; Ahmed, F.; Gan, Z.; Cheng, Y.; and Liu, J. 2019. UNITER: Learning Universal Image-Text Representations. *arXiv preprint arXiv:1909.11740*.
- Chiang, W.-L.; Li, Z.; and et al. 2023. Vicuna: An open-source chatbot impressing GPT-4 with 90% ChatGPT quality. See <https://vicuna.lmsys.org> (accessed 14 April 2023).
- Cui, C.; Zhou, Y.; Yang, X.; Wu, S.; Zhang, L.; Zou, J.; and Yao, H. 2023. Holistic Analysis of Hallucination in GPT-4V (ision): Bias and Interference Challenges. *arXiv preprint arXiv:2311.03287*.
- Dai, W.; Li, J.; Li, D.; Tiong, A. M. H.; Zhao, J.; Wang, W.; Li, B.; Fung, P. N.; and Hoi, S. 2024. InstructBLIP: Towards General-Purpose Vision-Language Models with Instruction Tuning. *Advances in Neural Information Processing Systems*, 36.
- Devlin, J.; Chang, M.-W.; Lee, K.; and Toutanova, K. 2018. BERT: Pre-training of Deep Bidirectional Transformers for Language Understanding. *arXiv preprint arXiv:1810.04805*.
- Fu, C.; Chen, P.; Shen, Y.; Qin, Y.; Zhang, M.; Lin, X.; Yang, J.; Zheng, X.; Li, K.; Sun, X.; Wu, Y.; and Ji, R. 2024. MME: A Comprehensive Evaluation Benchmark for Multi-modal Large Language Models. *arXiv:2306.13394*.
- Gilardi, F.; Alizadeh, M.; and Kubli, M. 2023. ChatGPT Outperforms Crowd-Workers for Text-Annotation Tasks. *arXiv preprint arXiv:2303.15056*.
- Guan, T.; Liu, F.; Wu, X.; Xian, R.; Li, Z.; Liu, X.; Wang, X.; Chen, L.; Huang, F.; Yacoob, Y.; et al. 2023. HallusionBench: An Advanced Diagnostic Suite for Entangled Language Hallucination & Visual Illusion in Large Vision-Language Models. *arXiv preprint arXiv:2310.14566*.
- Huang, Q.; Dong, X.; Zhang, P.; Wang, B.; He, C.; Wang, J.; Lin, D.; Zhang, W.; and Yu, N. 2023. Opera: Alleviating hallucination in multi-modal large language models via over-trust penalty and retrospection-allocation. *arXiv preprint, arXiv:2311.17911*.
- Huo, F.; Xu, W.; Zhang, Z.; Wang, H.; Chen, Z.; and Zhao, P. 2024. Self-introspective decoding: Alleviating hallucinations for large vision-language models. *arXiv preprint, arXiv:2408.02032*.
- Jia, C.; Yang, Y.; Xia, Y.; Chen, Y.-T.; Parekh, Z.; Pham, H.; Le, Q.; Sung, Y.-H.; Li, Z.; and Duerig, T. 2021. Scaling Up Visual and Vision-Language Representation Learning with Noisy Text Supervision. In *International Conference on Machine Learning (ICML)*, 4904–4916. PMLR.
- Lee, S.; Park, S. H.; Jo, Y.; and Seo, M. 2023. Volcano: Mitigating Multimodal Hallucination through Self-Feedback Guided Revision. *arXiv preprint arXiv:2311.07362*.
- Leng, S.; Zhang, H.; Chen, G.; Li, X.; Lu, S.; Miao, C.; and Bing, L. 2023. Mitigating object hallucinations in large vision-language models through visual contrastive decoding. *arXiv preprint, arXiv:2311.16922*.
- Li, Y.; Du, Y.; Zhou, K.; Wang, J.; Zhao, W. X.; and Wen, J.-R. 2023a. Evaluating Object Hallucination in Large Vision-Language Models. *arXiv preprint, arXiv:2305.10355*.
- Li, Y.; Du, Y.; Zhou, K.; Wang, J.; Zhao, W. X.; and Wen, J.-R. 2023b. Evaluating Object Hallucination in Large Vision-Language Models. *arXiv preprint arXiv:2305.10355*.
- Lin, T.-Y.; Maire, M.; Belongie, S.; Hays, J.; Perona, P.; Ramanan, D.; Dollár, P.; and Zitnick, C. L. 2014. Microsoft COCO: Common Objects in Context. In *Computer Vision—ECCV 2014: 13th European Conference, Zurich, Switzerland, September 6–12, 2014, Proceedings, Part V*, volume 8693 of *Lecture Notes in Computer Science*, 740–755. Springer.
- Liu, F.; Lin, K.; Li, L.; Wang, J.; Yacoob, Y.; and Wang, L. 2024a. Mitigating Hallucination in Large Multi-Modal Models via Robust Instruction Tuning. In *The Twelfth International Conference on Learning Representations*.
- Liu, H.; Li, C.; Li, Y.; Li, B.; Zhang, Y.; Shen, S.; and Lee, Y. J. 2024b. LLaVA-NeXT: Improved reasoning, OCR, and world knowledge.
- Liu, H.; Li, C.; Wu, Q.; and Lee, Y. J. 2024c. Visual instruction tuning. *Advances in Neural Information Processing Systems*, 36.

- Liu, H.; Xue, W.; Chen, Y.; Chen, D.; Zhao, X.; Wang, K.; Hou, L.; Li, R.; and Peng, W. 2024d. A Survey on Hallucination in Large Vision-Language Models. *arXiv preprint arXiv:2402.00253*.
- Lu, J.; Batra, D.; Parikh, D.; and Lee, S. 2019. ViLBERT: Pretraining Task-Agnostic Visiolinguistic Representations for Vision-and-Language Tasks. In *Advances in Neural Information Processing Systems (NeurIPS)*, volume 32.
- Nie, J.; Zhang, G.; An, W.; Tan, Y.-P.; Kot, A. C.; and Lu, S. 2024. MMREL: A Relation Understanding Dataset and Benchmark in the MLLM Era. *arXiv preprint arXiv:2406.09121*.
- Peng, Z.; Wang, W.; Dong, L.; Hao, Y.; Huang, S.; Ma, S.; and Wei, F. 2023. Kosmos-2: Grounding Multimodal Large Language Models to the World. *arXiv preprint arXiv:2306.14824*.
- Platt, J. C. 1999. Probabilistic outputs for support vector machines and comparisons to regularized likelihood methods. In *Advances in Large Margin Classifiers*, 61–74. MIT Press.
- Radford, A.; Kim, J. W.; Hallacy, C.; Ramesh, A.; Goh, G.; Agarwal, S.; Sastry, G.; Askell, A.; Mishkin, P.; Clark, J.; Krueger, G.; and Sutskever, I. 2021. Learning transferable visual models from natural language supervision. In *Proceedings of the International Conference on Machine Learning*, 8748–8763. PMLR.
- Raffel, C.; Shazeer, N.; Roberts, A.; Lee, K.; Narang, S.; Matena, M.; Zhou, Y.; Li, W.; and Liu, P. J. 2020. Exploring the Limits of Transfer Learning with a Unified Text-to-Text Transformer. *The Journal of Machine Learning Research*, 21(1): 5485–5551.
- Rohrbach, A.; Hendricks, L. A.; Burns, K.; Darrell, T.; and Saenko, K. 2018. Object Hallucination in Image Captioning. In *Proceedings of the 2018 Conference on Empirical Methods in Natural Language Processing (EMNLP)*, 4035–4045.
- Schwenk, D.; Khandelwal, A.; Clark, C.; Marino, K.; and Mottaghi, R. 2022. A-OKVQA: A Benchmark for Visual Question Answering Using World Knowledge. In *European Conference on Computer Vision*, 146–162. Springer.
- Shang, Y.; Cai, M.; et al. 2024. Llava-PruMerge: Adaptive token reduction for efficient large multimodal models. *arXiv preprint arXiv:2403.15388*.
- Sun, Z.; Shen, S.; Cao, S.; Liu, H.; Li, C.; Shen, Y.; Gan, C.; Gui, L.; Wang, Y.-X.; Yang, Y.; et al. 2023. Aligning Large Multimodal Models with Factually Augmented RLHF. *arXiv preprint arXiv:2309.14525*.
- Tan, H.; and Bansal, M. 2019. LXMERT: Learning Cross-Modality Encoder Representations from Transformers. *arXiv preprint arXiv:1908.07490*.
- Taori, R.; Gulrajani, I.; Zhang, T.; Dubois, Y.; Li, X.; Guestrin, C.; Liang, P.; and Hashimoto, T. B. 2023. Stanford Alpaca: An Instruction-Following LLaMA Model. https://github.com/tatsu-lab/stanford_alpaca.
- Touvron, H.; Martin, L.; and et al. 2023. Llama 2: Open foundation and fine-tuned chat models. *arXiv preprint arXiv:2307.09288*.
- Wang, X.; Zhou, Y.; Liu, X.; Lu, H.; Xu, Y.; He, F.; Yoon, J.; Lu, T.; Bertasius, G.; Bansal, M.; et al. 2024. MEMEN-TOS: A Comprehensive Benchmark for Multimodal Large Language Model Reasoning over Image Sequences. *arXiv preprint arXiv:2401.10529*.
- Wu, Z.; Xiong, Y.; Yu, S. X.; and Lin, D. 2018. Unsupervised Feature Learning via Non-Parametric Instance Discrimination. In *Proceedings of the IEEE Conference on Computer Vision and Pattern Recognition*, 3733–3742.
- Xing, Y.; Li, Y.; Laptev, I.; and Lu, S. 2024. Mitigating Object Hallucination via Concentric Causal Attention. *arXiv preprint, arXiv:2410.15926*.
- Ye, Q.; Xu, H.; Ye, J.; Yan, M.; Hu, A.; Liu, H.; et al. 2024. MPLUG-OWL2: Revolutionizing Multi-modal Large Language Model with Modality Collaboration. In *Proceedings of the IEEE/CVF Conference on Computer Vision and Pattern Recognition (CVPR)*, 13040–13051.
- Yin, S.; Fu, C.; Zhao, S.; Xu, T.; Wang, H.; Sui, D.; Shen, Y.; Li, K.; Sun, X.; and Chen, E. 2023. Woodpecker: Hallucination Correction for Multimodal Large Language Models. *arXiv preprint, arXiv:2310.16045*.
- You, H.; Zhang, H.; Gan, Z.; Du, X.; Zhang, B.; Wang, Z.; Cao, L.; Chang, S.-F.; and Yang, Y. 2023. Ferret: Refer and Ground Anything Anywhere at Any Granularity. *arXiv preprint arXiv:2310.07704*.
- Yu, Q.; Li, J.; Wei, L.; Pang, L.; Ye, W.; Qin, B.; and Zhuang, Y. 2024. HalluciDoctor: Mitigating Hallucinatory Toxicity in Visual Instruction Data. In *Proceedings of the IEEE/CVF Conference on Computer Vision and Pattern Recognition*, 12944–12953.
- Zhang, S.; Sun, P.; Chen, S.; Xiao, M.; Shao, W.; Zhang, W.; Chen, K.; and Luo, P. 2023a. GPT4RoI: Instruction Tuning Large Language Model on Region-of-Interest. *arXiv preprint arXiv:2307.03601*.
- Zhang, Y.; Qian, S.; Peng, B.; Liu, S.; and Jia, J. 2023b. Prompt Highlighter: Interactive Control for Multi-Modal LLMs. *arXiv preprint arXiv:2312.04302*.
- Zhou, Y.; Cui, C.; Yoon, J.; Zhang, L.; Deng, Z.; Finn, C.; Bansal, M.; and Yao, H. 2024. Analyzing and Mitigating Object Hallucination in Large Vision-Language Models. In *The Twelfth International Conference on Learning Representations*.
- Zhu, D.; Chen, J.; Shen, X.; Li, X.; and Elhoseiny, M. 2023. MiniGPT-4: Enhancing Vision-Language Understanding with Advanced Large Language Models. *arXiv preprint arXiv:2304.10592*.